metals

MDPI

Article

Study on the Microscopic Mechanism of Axle Steel EA4T during Uniaxial Cyclic Deformation Process

Xuehong Ren [1], Shaopu Yang [2,*], Wenjie Zhao [3] and Guilin Wen [1]

[1] State Key Laboratory of Advanced Design and Manufacturing for Vehicle Body, Hunan University, Changsha 410082, China
[2] State Key Laboratory of Mechanical Behavior in Traffic Engineering Structure and System Safety, Shijiazhuang Tiedao University, Shijiazhuang 050043, China
[3] School of Mechanical Engineering, Tianjin Sino-German University of Applied Sciences, Tianjin 300350, China
* Correspondence: yangsp@stdu.edu.cn

Abstract: In order to reveal the dislocation evolution law of body-centered cubic axle steel EA4T during cyclic deformation and provide an experimental basis for the subsequent construction of cyclic constitutive models based on microscopic physical mechanisms, macroscopic deformation experiments were first conducted on axle steel EA4T, including monotonic tensile experiments under different deformation amounts, symmetric strain cycling experiments under a different number of cycles, and ratcheting deformation experiments under a different number of cycles. Then, systematic observations of different samples at different deformation stages were conducted using a Transmission Electron Microscope (TEM) to investigate the dislocation configuration and evolution during strain cycling and ratcheting deformation. The observed results show that the dislocation evolution law of axle steel EA4T during the uniaxial tensile experiment, symmetrical strain cycling, and ratcheting deformation is basically the same, and the dislocation density increases with the increase in plastic deformation and number of cycles. The dislocation configuration gradually develops from low-density dislocation configurations such as dislocation lines and dislocation pileups to high-density dislocation configurations such as severe dislocation tangles and dislocation walls. The microscopic mechanism of the uniaxial ratcheting evolution of axle steel EA4T can be qualitatively explained by the dislocation configuration and evolution.

Keywords: axle steel EA4T; dislocation configuration; cyclic deformation; microscopic mechanism

check for updates

Citation: Ren, X.; Yang, S.; Zhao, W.; Wen, G. Study on the Microscopic Mechanism of Axle Steel EA4T during Uniaxial Cyclic Deformation Process. *Metals* **2023**, *13*, 1379. https://doi.org/10.3390/met13081379

Academic Editor: Atef Saad Hamada

Received: 16 June 2023
Revised: 20 July 2023
Accepted: 27 July 2023
Published: 31 July 2023

Copyright: © 2023 by the authors. Licensee MDPI, Basel, Switzerland. This article is an open access article distributed under the terms and conditions of the Creative Commons Attribution (CC BY) license (https://creativecommons.org/licenses/by/4.0/).

1. Introduction

The accumulation of strain caused by cyclic loading is very important in structural component design and mechanical engineering. Ratcheting refers to the accumulation of plastic deformation that occurs in a material during asymmetric stress cycles. Engineering components inevitably bear asymmetric stress cyclic loadings during actual work processes. Conducting research on ratcheting behavior is very important in structural component design and mechanical engineering and has important engineering significance and academic value. Many researchers have conducted comprehensive and in-depth research on the ratcheting effect from both experimental and theoretical perspectives, as reviewed by Ohno [1,2], Kang [3], Chaboche [4], and Sun [5], and more recently by Zhao [6], Kan [7], Kang [8], Xu [9], MOSLEMI [10], Bai [11], and Xu L [12] et al.

However, these models are mostly macroscopic phenomenological cyclic constitutive models established based on macroscopic experiments. The macroscopic cyclic constitutive model does not include the microscopic physical mechanism of cyclic deformation, requiring the introduction of response evolution equations and a large number of material parameters, greatly limiting the engineering application of such cyclic constitutive models. As is well known, the microscopic physical mechanisms of plastic deformation in face-centered cubic (FCC) and body-centered cubic (BCC) metals at room temperature

are mainly attributed to dislocation slip in active slip systems. In order to include as much microphysical information about cyclic deformation as possible in the constitutive model, cyclic polycrystalline constitutive models based on crystal plasticity have recently been attempted and developed by Guo [13], Dong [14,15], Ren [16,17], Lei [18], Li [19], and so on. The establishment of crystal plastic constitutive models provides a new option for improving the ability to predict ratcheting deformation. However, the establishment and improvement of these models require a comprehensive understanding of the formation and evolution of dislocation morphology during cyclic and ratcheting deformation.

In order to reveal the micro-mechanism of cyclic deformation, a series of experimental studies were conducted. Buque et al. [20] (2001), El Madhoun et al. [21] (2003), Zhang and Jiang [22] (2005), Feaugas et al. [23] (2008), and Taleb and Hauet [24] (2009) studied the microscopic mechanisms of cyclic plastic deformation by observing the dislocation configuration and their evolution during the cyclic deformation of FCC polycrystalline metals. However, these microscopic observations only focus on the strain-cyclic loading of the material rather than the ratcheting deformation under asymmetric stress-controlled cyclic loading.

Bocher et al. [25] and Feaugas and Gaudin [26,27] observed the dislocation structure of 316 stainless steel after ratcheting deformation under different experimental conditions, qualitatively explaining that the formation of inhomogeneous polarized dislocation substructures composed of dislocation walls and dislocation cells from the cross slip of screw dislocations is the microscopic physical mechanism of ratcheting deformation. However, the dislocation patterns are mainly observed at the end of cyclic loading, and the evolution of dislocations at different stages of ratcheting deformation has not been studied in detail.

Cheng et al. [28] observed the microstructure evolution of 304 stainless steel during uniaxial ratcheting deformation and found that when the ratcheting strain reached a certain value, the strain-induced Martensite transformation occurred during the ratcheting process, and the amount of induced Martensite gradually increased with the number of cycles. In order to reveal the microscopic mechanism of ratcheting deformation, Dong et al. [29–31] and Kang et al. [32,33] recently observed the dislocation structures and their evolution law of metals with different crystal structures during uniaxial ratcheting and multiaxial ratcheting through transmission electron microscopy (TEM). It was found that during the ratcheting deformation process, the dislocation configuration gradually evolves from low-density dislocation configurations such as dislocation lines and dislocation pileups to high-density dislocation configurations such as dislocation veins, dislocation walls, and dislocation cells as the number of cycles increases.

However, there is relatively little research on the microscopic mechanism of metal ratcheting deformation, especially for metals with different crystal structures (such as body centered cubic structure metals) and different cyclic softening metal materials. Further in-depth research is still needed to obtain the microscopic mechanism of material cyclic deformation.

Therefore, it is necessary to conduct microscopic observations on dislocation configuration and its evolution during the cyclic plastic deformation of face-centered cubic and body-centered cubic polycrystalline metals in order to reasonably reveal the microscopic mechanisms of metal cyclic plastic deformation. These microscopic mechanisms are very important for constructing cyclic plastic constitutive models based on micro-mechanisms.

This paper will study the microscopic mechanism of EA4T axle steel during cyclic deformation based on the macroscopic experimental research on cyclic deformation in the research group [34] in order to provide experimental support and theoretical basis for the subsequent construction of cyclic constitutive models based on micro-physical mechanisms.

The specific research content of this paper is as follows: Firstly, macroscopic deformation experiments were conducted on axle steel EA4T, including monotonic tensile experiments under different deformation amounts, symmetric strain cycling experiments under different number of cycles, and uniaxial ratcheting deformation experiments under a different number of cycles. Then, a systematic observation of different samples at different

deformation stages was conducted using a Transmission Electron Microscope (TEM) to investigate the dislocation configuration and evolution during strain cycling and ratcheting deformation at different deformation stages. Finally, the micro-physical mechanism of the cyclic deformation of axle steel EA4T is summarized and discussed. At the same time, the microscopic mechanism of the uniaxial ratcheting evolution of axle steel EA4T can be qualitatively explained by the dislocation configuration and evolution.

2. Macroscopic Deformation Experiment of Axle Steel EA4T

Axle steel EA4T (25CrMo4 steel) is a low-carbon alloy steel produced by Germany's Siemens company and is widely used in hollow axles of high-speed trains. Its main chemical composition is shown in Table 1.

Table 1. Main Chemical Composition of Axle Steel EA4T (Mass Fraction%).

C	Mn	Si	Cr	Mo	Ni	V	S	P	Cu
0.22~0.29	0.5~0.8	0.15~0.40	0.90~1.20	0.15~0.3	0.3	0.06	0.015	0.02	0.3

The instrument used in the macroscopic deformation experiment of this paper is the MTS810 material fatigue testing machine (MTS Systems Corporation, Eden Prairie, MN, USA). The uniaxial deformation experiment requires processing the material into a solid round bar specimen, with the specific shape and processing dimensions shown in Figure 1. Three sets of experiments were conducted on axle steel EA4T at room temperature, including monotonic tensile experiments under different deformation amounts, symmetric strain cycling experiments under a different number of cycles, and ratcheting deformation experiments under a different number of cycles. The main experimental conditions are shown in Table 2.

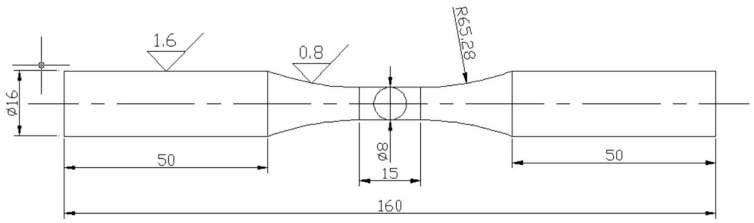

Figure 1. Shape and machining dimensions of uniaxial specimens (unit: mm).

Table 2. Experimental Conditions of Axle Steel EA4T.

Experimental Conditions	Number	Experimental Conditions	Loading Rate	Number of Cycles
Uniaxial tensile experiment	1	Tension to 5%	2×10^{-3}/s	
	2	Tension to 8%	2×10^{-3}/s	
Symmetrical strain cycling experiment	3	±0.7%	2×10^{-3}/s	50 Cycle
	4	±0.7%	2×10^{-3}/s	300 Cycle
Uniaxial ratcheting deformation experiment	5	75 ± 475 MPa	50 MPa/s	30 Cycle
	6	75 ± 475 MPa	50 MPa/s	110 Cycle

Figure 2 shows the uniaxial tensile curves (i.e., engineering stress-strain curves) of axle steel EA4T under different deformations (5% and 8%) at a strain rate of 2×10^{-3}/s. It can be seen that different uniaxial tensile curves almost overlap, indicating that the materials of different samples are basically the same, and the experiment has good repeatability, which can ensure the effectiveness of microscopic TEM experiments.

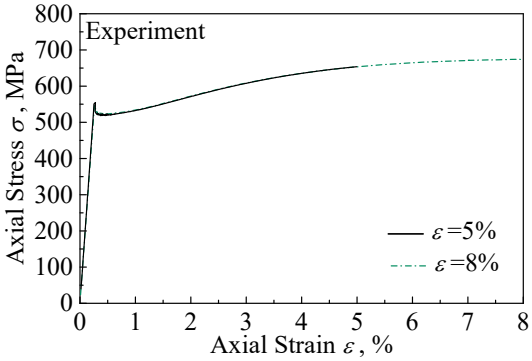

Figure 2. Experimental results of axle steel EA4T uniaxial tensile curve.

Meanwhile, through experimental curves, it can be seen that the axle steel EA4T has a brief yield plateau at the initial yield point, followed by a significant strain hardening phenomenon. The strength limit of axle steel is about 660 MPa, with an upper yield strength of about 550 MPa and a lower yield strength of about 520 MPa.

Figure 3 shows the experimental results of axle steel EA4T under symmetric strain cycling at a strain loading rate of 2×10^{-3}/s with a strain amplitude of ±0.7%, where Figure 3a,b show the cyclic stress-strain curves at different cycles of axle steel EA4T, and Figure 3c shows the relationship curve between the responsive stress amplitude and the number of cycles under different cycles. The number of cycles is set to 50 and 300, respectively.

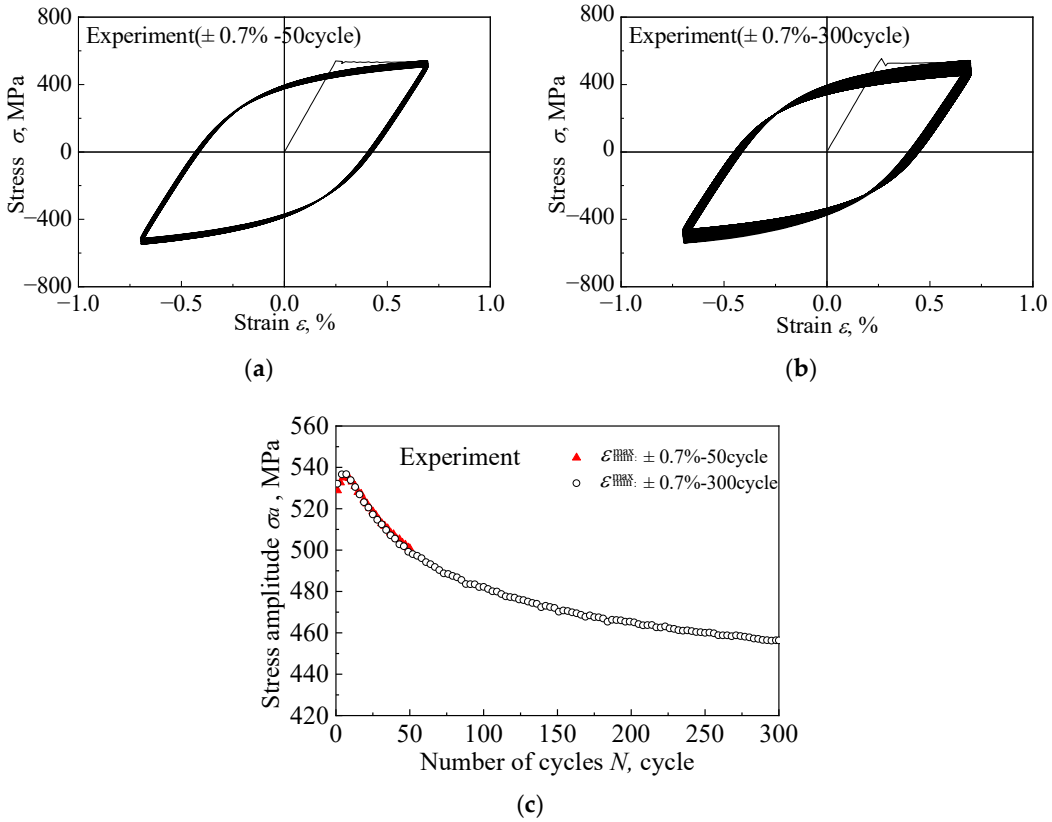

Figure 3. Symmetric strain cycling experiment results of axle steel EA4T under different number of cycles: (**a**) cyclic stress-strain curve (50 cycles); (**b**) cyclic stress-strain curve (300 cycles); (**c**) The relationship curve between the responsive stress amplitude and the number of cycles.

In strain cycling experiments, the definition of the responsive stress amplitude is: $\sigma_a = (\sigma_{max} + \sigma_{min})/2$. In the equation, σ_{max} and σ_{min} are the values of the maximum

and minimum responsive stresses corresponding to the symmetric strain cycling experiment, respectively.

From Figure 3, it can be seen that the axle steel EA4T exhibits cyclic softening characteristics in the strain-controlled cycling experiment, that is, the responsive stress amplitude σ_a will gradually decrease with the increase in the number of cycles. At the same time, it can also be seen that the rate of cyclic softening of axle steel EA4T gradually decreases with the number of cycles, and there is no saturation phenomenon of cyclic softening within the maximum number of cycles specified in the experiment.

Meanwhile, it can also be seen that the evolution curves of responsive stress amplitude under different number of cycles almost overlap, indicating that the material has less dispersion and the repeatability of the experiment is strong.

Figure 4 shows the evolution curve of ratcheting strain of axle steel EA4T under a different number of cycles with a mean stress of 75 MPa and a stress amplitude of 475 MPa, where Figure 4a,b show the experimental results of stress-strain hysteresis loops under a different number of cycles, and Figure 4c shows the evolution curves of uniaxial ratcheting strain at a different number of cycles. The number of cycles is, respectively, set to 30 and 110, with a loading stress rate of 50 MPa/s.

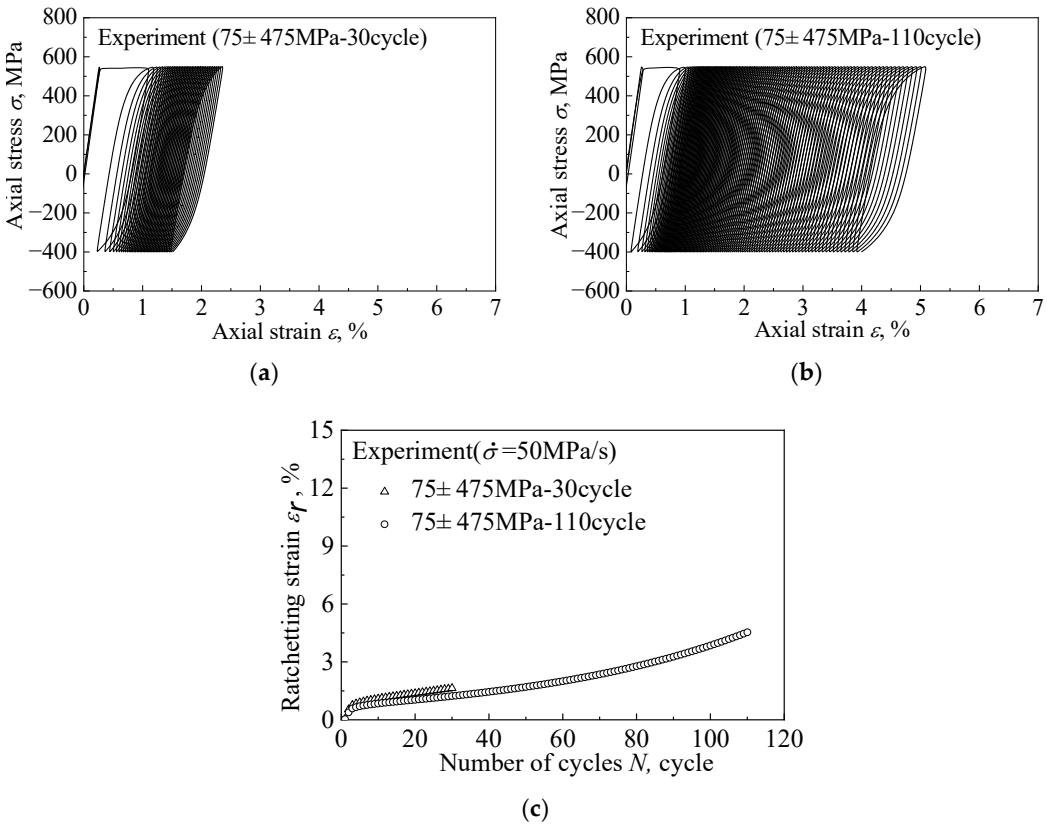

Figure 4. Evolution curve of ratcheting strain of axle steel EA4T under different number of cycles: (**a**) stress-strain hysteresis loop curve (30 cycles); (**b**) stress-strain hysteresis loop curve (110 cycles); (**c**) evolution curve of uniaxial ratcheting strain.

In asymmetric stress cycles, the definition of ratcheting strain is: $\varepsilon_r = (\varepsilon_{max} + \varepsilon_{min})/2$. In the equation, ε_{max} and ε_{min}, are the maximum and minimum strain values in the asymmetric stress cycling experiment, respectively. From the experimental results, it can be seen that the evolution curves of the ratcheting strain of axle steel EA4T under a different number of cycles tend to be basically consistent, indicating that the material dispersion is very small and the experiment has good repeatability.

From Figure 4a,b, it can be seen that the stress–strain hysteresis loop of axle steel EA4T exhibits an evolution trend from narrow to wide during the uniaxial ratcheting deformation process, mainly because axle steel EA4T belongs to cyclic softening material.

At the same time, it can also be seen that the ratcheting strain of axle steel EA4T increases with the increase in cycling cycles during asymmetric stress cycling. According to the evolution trend of uniaxial ratcheting strain rate, the evolution curve of the uniaxial ratcheting strain of cyclic softening axle steel EA4T can be divided into three stages: in the first stage, the ratcheting strain rate rapidly decreases from large to small with the number of cycles; in the second stage, the ratcheting strain rate remains constant; in the third stage, the ratcheting strain rate gradually increases, and the material enters the stage of instability and failure.

3. Microscopic Mechanism of Axle Steel EA4T during Cyclic Deformation

After the macroscopic deformation experiments, the solid round bar specimen is cut along the direction parallel to the axis in the gauge length section. Then, it is cut into thin sheets with a thickness of 0.5 mm using a wire cutting machine and four samples are taken from each sample. After the wire cutting is completed, metallographic sandpaper from coarse to fine is used for polishing, and, finally, to 30–40 um is polished. Then, the ground sample is cut into circular discs with a diameter of 3 mm using a punching machine, and electrolytic double spraying is performed on the ground sample. Perchloric acid alcohol solution with a concentration of 15% is selected as the electrolytic double spray solution. The Transmission Electron Microscope (T EM) experiment uses the Transmission Electron Microscope (TEM) JEM-2100 produced by JEOL company in Japan. The Transmission Electron Microscope (TEM) was used to systematically observe the dislocation configuration of thin film samples under each experimental condition, and rough statistical analysis was conducted to summarize the dislocation evolution law of the material during monotonic tensile and cyclic deformation.

It should be noted that the plastic deformation of polycrystals is inhomogeneous at the grain scale due to the different crystal orientations between grains. The main dislocation configuration presented under each experimental condition in this article is the result of rough statistical analysis of the dislocation morphology of many grains in four thin film samples.

3.1. Dislocation Evolution Law in Uniaxial Tension

Firstly, Figure 5 shows the metallographic structure photos of axle steel EA4T before deformation. It can be seen that the original structure of axle steel EA4T before deformation is mainly composed of tempered Martensite and Bainite.

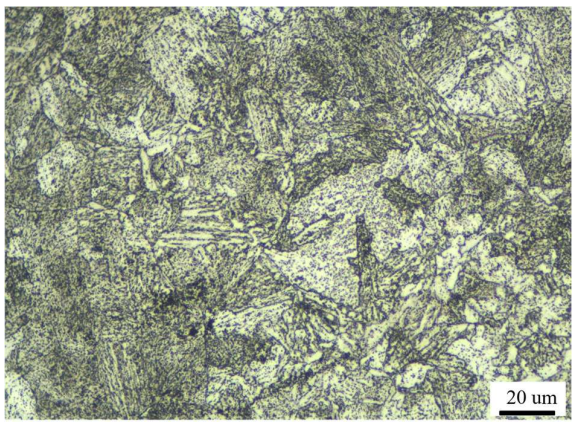

Figure 5. Original microstructure of axle steel EA4T before deformation.

The original dislocation configuration of body-centered cubic axle steel EA4T before deformation was observed using TEM, as shown in Figure 6. It can be seen that the disloca-

tion density in the original sample is relatively low, and the main dislocation configuration is discrete dislocation lines, as shown in Figure 6a. Some dislocation pileup can be observed near the grain boundary, but the dislocation density is low, as shown in Figure 6b.

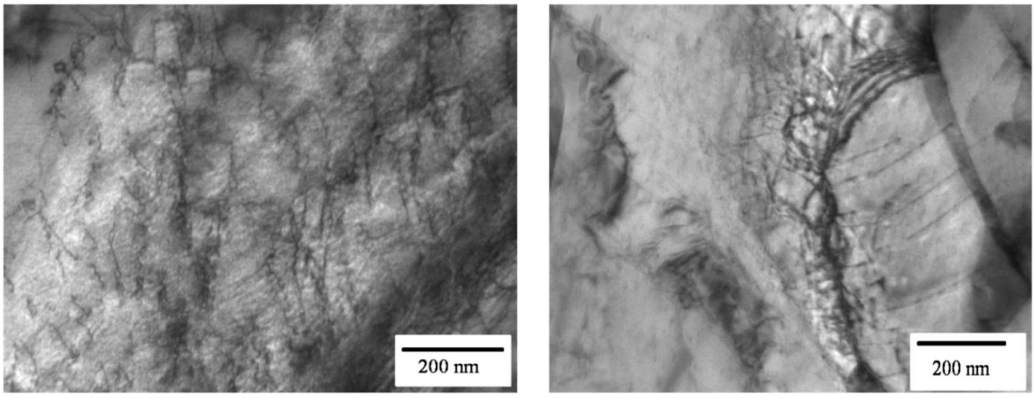

(**a**) (**b**)

Figure 6. Original dislocation configuration of axle steel EA4T before deformation: (**a**) discrete dislocation lines; (**b**) dislocation pileup.

In order to compare and analyze the dislocation evolution law of axle steel EA4T during strain cycling and ratcheting deformation, the dislocation configuration of body-centered cubic (BCC) axle steel EA4T of uniaxial tension under different deformation amounts was first observed. Figures 7 and 8 show the dislocation configuration of body-centered cubic structure axle steel EA4T under tensile deformation of 5% and 8%, respectively.

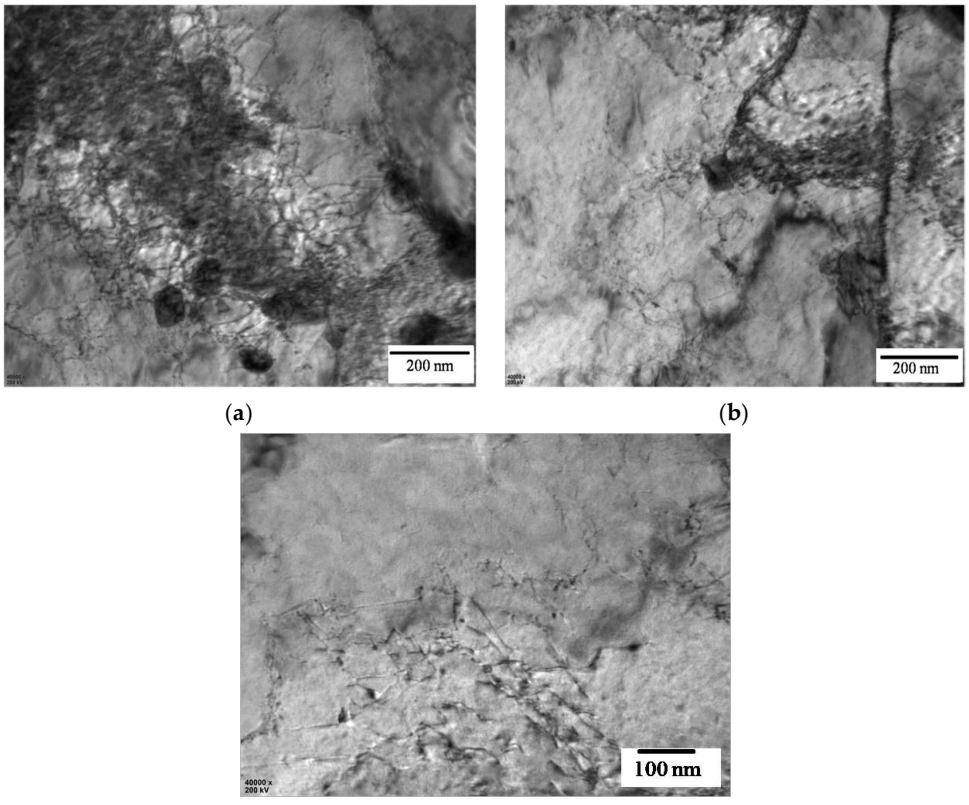

(**a**) (**b**)

(**c**)

Figure 7. The main dislocation configuration of axle steel EA4T with a uniaxial tensile deformation of 5%: (**a**) dislocation tangles; (**b**) dislocation pileup; (**c**) dislocation lines.

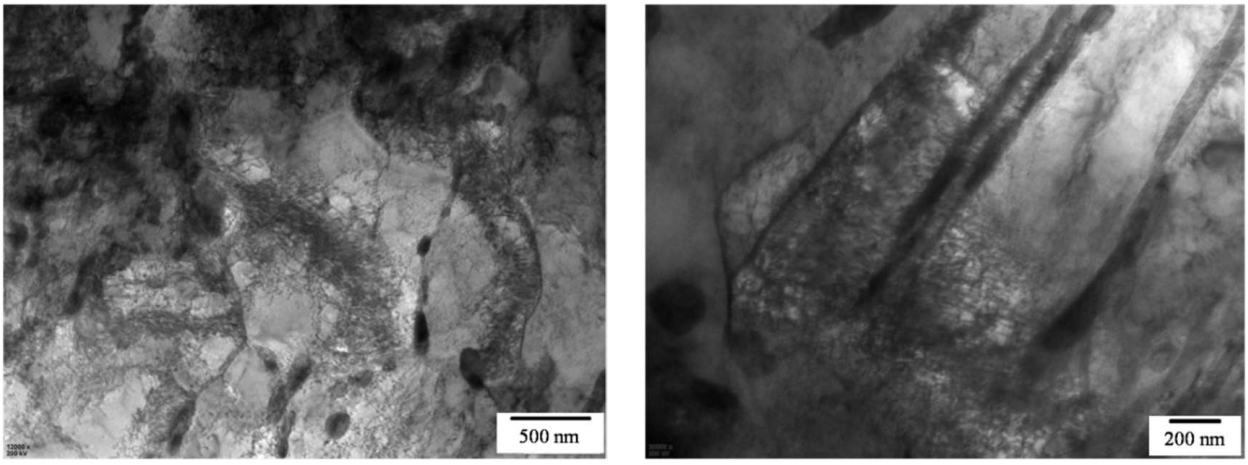

(**a**) (**b**)

Figure 8. The main dislocation configuration of axle steel EA4T with a uniaxial tensile deformation of 8%: (**a**) severe dislocation tangles; (**b**) dislocation tangles and dislocation wall.

From the analysis of the results, it can be seen that:

(1) when the uniaxial tensile deformation is 5%, the main dislocation configuration can be observed by the Transmission Electron Microscope (TEM) as dislocation tangles, as shown in Figure 7a. Meanwhile, dislocation pileup can be observed at the grain boundaries, as shown in Figure 7b. When the deformation of uniaxial tension reaches 8%, the main dislocation configuration is high-density dislocation tangle, as shown in Figure 8a, where a small portion of grains have a tendency to form dislocation walls, as shown in Figure 8b.

(2) During the tensile deformation, dislocations multiply continuously through a typical mechanism, and the dislocation density significantly increases with the increase in tensile plastic deformation. The dislocation configuration gradually develops from low-density dislocation configurations, such as dislocation lines and dislocation pileups, to high-density dislocation configurations, such as severe dislocation tangles and dislocation walls;

(3) The plastic deformation of polycrystalline metal is inhomogeneous at the grain scale, taking the tensile deformation of 5% as an example. Specifically, dislocation tangles and dislocation pileup can be observed in most grains, as shown in Figure 7a,b. However, in a small part of grains, only dislocation lines or dislocation-free zones can be observed, as shown in Figure 7c. This is mainly caused by different crystal orientations, which can be seen in references [30,33].

3.2. The Evolution Law of Dislocations during Ratcheting Deformation

Then, the dislocation configuration of body-centered cubic axle steel EA4T during uniaxial ratcheting deformation (mean stress 75 MPa, stress amplitude 475 MPa) was observed. Figures 9 and 10 show the main dislocation configuration of body-centered cubic axle steel EA4T at 30 and 110 cycles, respectively.

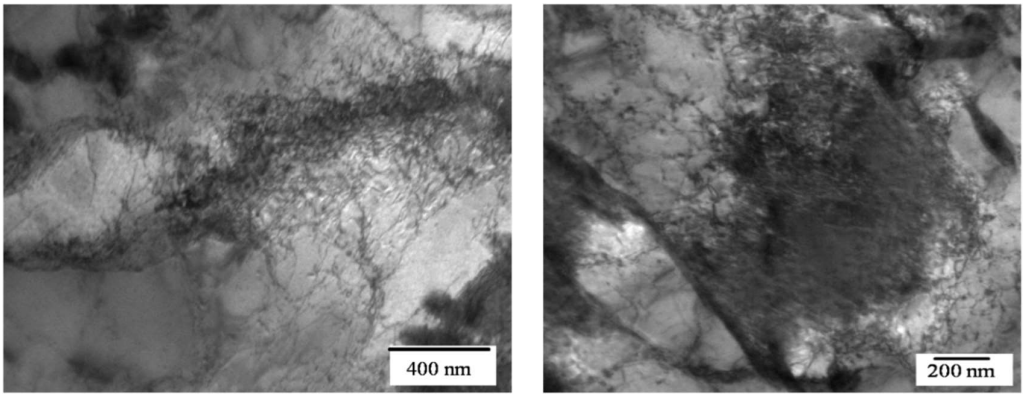

(**a**) (**b**)

Figure 9. The main dislocation configuration of axle steel EA4T during uniaxial ratcheting deformation with 30 cycles: (**a**) dislocation pileup; (**b**) dislocation tangles.

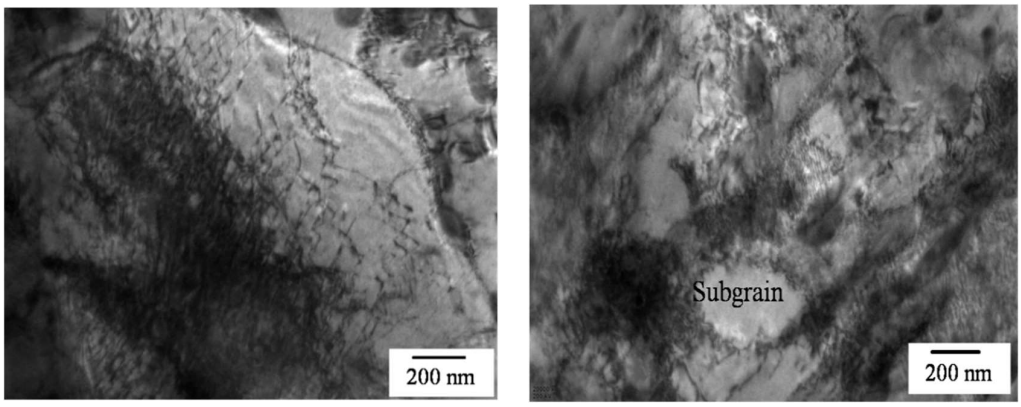

(**a**) (**b**)

Figure 10. The main dislocation configuration of axle steel EA4T during uniaxial ratcheting deformation with 110 cycles: (**a**) severe dislocation tangles; (**b**) dislocation tangles and early subgrain.

From the analysis of experimental results, it can be seen that:

(1) when the number of cycles is 30, the ratcheting deformation is 1.93%, and the main dislocation configurations of axle steel EA4T are dislocation tangles and dislocation pileup, as shown in Figure 9;
(2) when the cycle number is 110 cycles, the ratcheting deformation is 4.53%. The main dislocation configuration of axle steel EA4T is dislocation pileup, and some crystals generate severe dislocation tangles, as shown in Figure 10a; The dislocation cellular structure is not obvious, and very few grains have early sub-grains, as shown in Figure 10b.
(3) During the uniaxial ratcheting deformation of axle steel EA4T, dislocations are also constantly proliferating. The dislocation density gradually increases with the increase in the number of cycles and ratcheting strain, and a small portion of grains will form early subgrains in the later stage of the ratcheting deformation experiment.

Based on the observed evolution of dislocation configuration, the microscopic mechanism of the uniaxial ratcheting evolution of body-centered cubic axle steel EA4T can be qualitatively explained as follows:

(1) At the first stage and early second stage of ratcheting strain, i.e., when the number of cycles is less than 30, the main dislocation configuration of axle steel EA4T has evolved from discrete dislocation lines to complex dislocation configuration, such as dislocation tangles and dislocation pileup, with a rapid increase in dislocation

density. The increase in dislocation density and the formation of complex dislocation configurations during the initial stage of ratcheting deformation improved the degree of hardening of axle steel EA4T, resulting in a gradual decrease in ratcheting strain rate during the first stage.

(2) At the second stage of ratcheting strain, i.e., when the cycle of ratcheting strain is less than 110, although the dislocation density of axle steel EA4T increases, its main dislocation configuration is relatively stable and still forms dislocation tangles, resulting in a constant ratcheting strain rate at the second stage. However, the dislocation density in the second stage of the ratcheting strain is greater than that in the first stage, so the ratcheting strain rate in the second stage is smaller than that in the first stage.

3.3. The Evolution Law of Dislocations during Strain Cycling

Finally, the dislocation configuration of body-centered cubic steel EA4T during cyclic deformation controlled by symmetric strain (strain amplitude ±0.7%) was observed by transmission electron microscopy. Figures 11 and 12, respectively, show the dislocation configuration of axle steel EA4T at symmetrical strain cycles of 50 and 300 cycles, respectively.

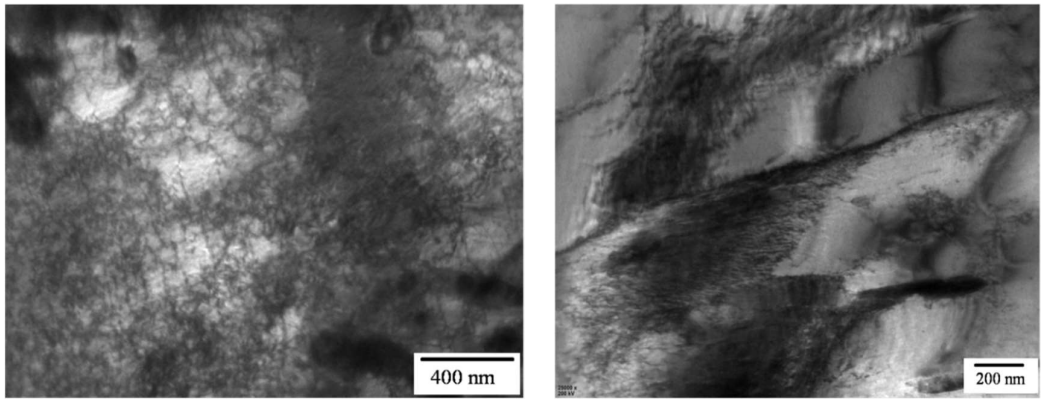

(**a**) (**b**)

Figure 11. The main dislocation configuration of axle steel EA4T during symmetrical strain cycling experiments at 50 cycles: (**a**) high-density dislocation tangles; (**b**) dislocation tangles and dislocation wall.

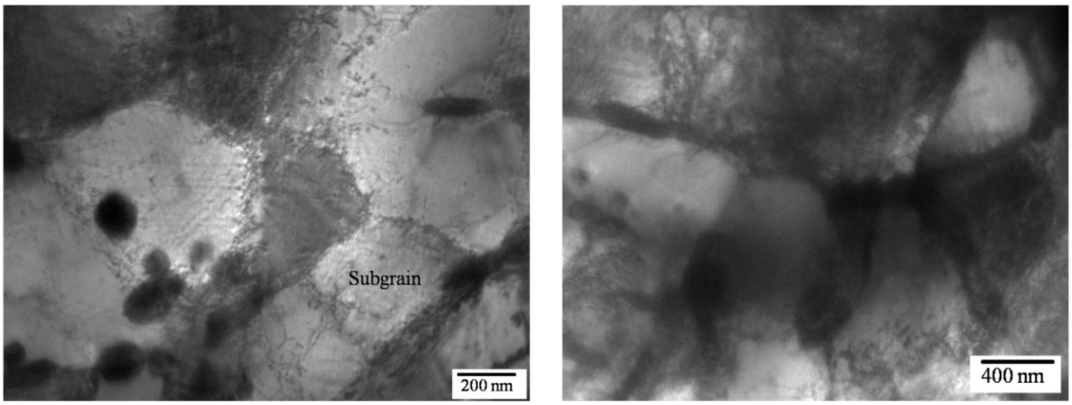

(**a**) (**b**)

Figure 12. The main dislocation configuration of axle steel EA4T during symmetrical strain cycling experiments at 300 cycles: (**a**) high-density dislocation tangles and subgrain; (**b**) subgrain.

From the experimental results, it can be concluded that:

(1) During the strain cycling process, the rate of dislocation multiplication is very fast. When the number of strain cycles is 50, the main dislocation configuration of axle steel EA4T is high-density dislocation tangles, as shown in Figure 11a. Dislocation walls with a tendency to form dislocation cells can be observed in certain grains, as shown in Figure 11b.
(2) When the number of strain cycling is 300, a large number of subgrains can be observed in the later stage of the strain cycling experiment [30,35], as shown in Figure 12.
(3) During the strain cycling of axle steel EA4T, the dislocation density gradually increases with the increase in the number of cycles. The rate of dislocation multiplication during the strain cycling is higher than that of dislocations during uniaxial ratcheting deformation. The dislocation configuration gradually forms a high-density inhomogeneous dislocation configuration from a low-density dislocation configuration, and finally tends to form a stable subgrain structure, similar to the stable dislocation configuration of body centered cubic polycrystalline 20 carbon steel [30,32].

4. Conclusions

This paper first conducted macroscopic monotonic tensile experiments under different deformation amounts, symmetric strain cyclic experiments under different number of cycles, and ratcheting deformation experiments under a number of cycles on axle steel EA4T. The Transmission Electron Microscope (TEM) was used to systematically observe the dislocation configuration of different samples at different deformation stages. Based on the comprehensive analysis of the macroscopic deformation experiment and Transmission Electron Microscope (TEM) experiment results of axle steel EA4T, the following conclusions can be drawn:

1. Axle steel EA4T exhibits cyclic softening characteristics in strain-controlled cycling experiments, that is, the responsive stress amplitude will gradually decrease with the increase in the number of cycles. At the same time, the rate of cyclic softening of axle steel EA4T gradually decreases with the number of cycles, and there is no saturation phenomenon of cyclic softening within the maximum cycle set in this experiment. The ratcheting strain of axle steel EA4T increases with the increase in cycling cycles during asymmetric stress cycling. According to the evolution trend of uniaxial ratcheting strain rate, the evolution curve of uniaxial ratcheting strain of axle steel EA4T can be divided into three stages: in the first stage, the ratcheting strain rate rapidly decreases from large to small with the number of cycles, while in the second stage, the ratcheting strain rate remains constant. In the third stage, the ratcheting strain rate gradually increases, and the material enters the stage of instability and failure.
2. The dislocation evolution law of axle steel EA4T during the uniaxial tensile experiment, symmetrical strain cycling, and the ratcheting deformation experiment is basically the same, and the dislocation density increases with the increase in plastic deformation and the number of cycles. The dislocation configuration gradually develops from low-density dislocation configurations such as dislocation lines and dislocation pileups to high-density dislocation configurations such as severe dislocation tangles and dislocation walls. A small portion of the grains will form early subgrains in the later stage of the ratcheting deformation experiment, and a large number of subgrains can be observed in the later stage of the strain cycling experiment. The rate of dislocation multiplication during strain cycling is faster than that during uniaxial ratcheting deformation.
3. Based on the observed dislocation configuration evolution, the microscopic mechanism of the uniaxial ratcheting evolution of body centered cubic axle steel EA4T can be qualitatively explained as follows: at the first stage and early second stage of ratcheting strain, the main dislocation configuration of axle steel EA4T has evolved from discrete dislocation lines to complex dislocation configuration, such as dislocation tangles and dislocation pileup. The increase in dislocation density and the formation of complex dislocation configurations during the initial stage of ratcheting deformation

improved the degree of hardening of axle steel EA4T, resulting in a gradual decrease in ratcheting strain rate during the first stage. At the second stage of ratcheting strain, although the dislocation density of axle steel EA4T increases, its main dislocation configuration is relatively stable and still forms dislocation tangles, resulting in a constant ratcheting strain rate at the second stage. However, the dislocation density in the second stage of the ratcheting strain is greater than that in the first stage, so the ratcheting strain rate in the second stage is smaller than that in the first stage.

Author Contributions: Conceptualization, X.R.; methodology, X.R.; software, X.R.; validation, X.R.; formal analysis, X.R.; investigation, W.Z.; resources, W.Z.; data curation, W.Z.; writing—original draft preparation, X.R.; writing—review and editing, X.R.; visualization, G.W.; supervision, S.Y.; project administration, S.Y.; funding acquisition, G.W. All authors have read and agreed to the published version of the manuscript.

Funding: The present work is supported by the National Natural Science Foundation of China (Nos.12032017, 11790282).

Data Availability Statement: Data will be made available on request.

Conflicts of Interest: The authors declare no conflict of interest.

References

1. Ohno, N. Recent topics in constitutive modeling of cyclic plasticity and viscoplasticity. *Appl. Mech. Rev.* **1990**, *43*, 283–295. [CrossRef]
2. Ohno, N. Recent progress in constitutive modeling for Ratcheting. *J. Soc. Mater. Sci. Jpn.* **1997**, *46*, 1–9. [CrossRef]
3. Kang, G. Ratcheting: Recent progresses in phenomenon observation, constitutive modeling and application. *Int. J. Fatigue* **2008**, *30*, 1448–1472. [CrossRef]
4. Chaboche, J.L. A review of some plasticity and visco-plasticity constitutive theories. *Int. J. Plast.* **2008**, *24*, 1642–1693. [CrossRef]
5. Sun, L.; Guo, S.; Yuan, G.; Chen, Y.; Zhang, X.; Tu, S. Macro/micro Cyclic Constitutive Models and Their Application in Engineering Structures. *J. Mech. Eng.* **2021**, *57*, 198–217.
6. Zhao, J.; Fu, P.; Xu, X.; Zhang, X.; Wang, P.; Kan, Q. A cyclic visco-plastic constitutive model for the ratcheting behavior of U75VG rail steel under a wide range of loading rates. *Eng. Fail. Anal.* **2022**, *138*, 106342. [CrossRef]
7. Kan, Q.; Zhao, J.; Xu, X.; Wang, Z.; Zhang, X.; Wang, P. Temperature-dependent cyclic plastic deformation of U75VG rail steel: Experiments and simulations. *Eng. Fail. Anal.* **2022**, *140*, 106527. [CrossRef]
8. Kang, G.; Kan, Q. Application of cyclic plasticity for modeling ratcheting in metals. In *Cyclic Plasticity of Metals*; Elsevier: Amsterdam, The Netherlands, 2022; pp. 325–355.
9. Xu, X.; Ding, L.; Miao, H.; Wen, Z.; Chen, R.; Kan, Q.; Kang, G. Nonproportionally multiaxial cyclic plastic deformation of U75 rail steel: Experiment and modeling. *Int. J. Fatigue* **2023**, *168*, 107480. [CrossRef]
10. Moslemi, N.; Mozafari, F.A.R.Z.İ.N.; Abdi, B.; Gohari, S.; Redzuan, N.; Burvill, C.; Ayob, A. Uniaxial and biaxial ratcheting behavior of pressurized AISI 316L pipe under cyclic loading: Experiment and simulation. *Int. J. Mech. Sci.* **2020**, *179*, 105693. [CrossRef]
11. Bai, J.; Jin, K.; Kou, Y. An improved kinematic hardening rule describing the effect of loading history on plastic modulus and ratcheting strain. *Acta Mech.* **2023**, *234*, 1757–1776. [CrossRef]
12. Xu, L.Y.; Fan, J.S.; Yang, Y.; Tao, M.X.; Tang, Z.Y. An improved elasto-plastic constitutive model for the exquisite description of stress-strain hysteresis loops with cyclic hardening and softening effects. *Mech. Mater.* **2020**, *150*, 103590. [CrossRef]
13. Guo, G.; Jiang, W.; Liu, X.; Chen, J.; Li, L.; Wang, J.; Zhang, Y.; Zhang, Z. In-situ SEM-EBSD investigation of the low-cycle fatigue deformation behavior of Inconel 718 at grain-scale. *J. Mater. Res. Technol.* **2023**, *24*, 5007–5023. [CrossRef]
14. Dong, Y.; Kang, G.; Yu, C. A dislocation-based cyclic polycrystalline visco-plastic constitutive model for ratchetting of metals with face-centered cubic crystal structure. *Comput. Mater. Sci.* **2014**, *91*, 75–82. [CrossRef]
15. Dong, Y.; He, X.; Zhang, Z. A new crystal plasticity modeling of uniaxial ratcheting behavior for face-centered cubic 6061 aluminum alloy. *Mater. Res. Express* **2020**, *7*, 106515. [CrossRef]
16. Ren, X.H.; Yang, S.P.; Wen, G.L.; Zhao, W.J. A Crystal-Plasticity Cyclic Constitutive Model for the Ratcheting of Polycrystalline Material Considering Dislocation Substructures. *Acta Mech. Solida Sin.* **2020**, *33*, 268–280. [CrossRef]
17. Ren, X.H.; Yang, S.P.; Zhao, W.J.; Wen, G.L. A crystal plasticity-based constitutive model for Ratcheting of cyclic hardening polycrystalline metals. *Int. J. Dyn. Control* **2020**, *8*, 1161–1168. [CrossRef]
18. Lei, Y.; Yu, C.; Wang, Z.; Xu, X.; Li, H.; Kang, G. Multi-mechanism constitutive model for uniaxial Ratcheting of extruded AZ31 magnesium alloy at room temperature. *Mech. Mater.* **2023**, *179*, 104607. [CrossRef]
19. Li, H.; Yu, C.; Kang, G. Crystal plasticity modeling of the multiaxial Ratcheting of extruded AZ31 Mg alloy. *Int. J. Plast.* **2022**, *152*, 103242. [CrossRef]

20. Buque, C.; Bretschneider, J.; Schwab, A.; Holste, C. Dislocation structures in cyclically deformed nickel polycrystals. *Mater. Sci. Eng. A* **2001**, *300*, 254–262. [CrossRef]
21. El-Madhoun, Y.; Mohamed, A.; Bassim, M.N. Cyclic stress-strain response and dislocation structures in polycrystalline aluminum. *Mater. Sci. Eng. A* **2003**, *359*, 220–227. [CrossRef]
22. Zhang, J.; Jiang, Y. An experimental investigation on cyclic plastic deformation and substructures of polycrystalline copper. *Int. J. Plast.* **2005**, *21*, 2191–2211. [CrossRef]
23. Feaugas, X.; Catalao, S.; Pilvin, P.; Cabrillat, M.T. On the evolution of cyclic deformation microstructure during relaxation test in austenitic stainless steel at 823K. *Mater. Sci. Eng. A* **2008**, *483*, 422–425. [CrossRef]
24. Taleb, L.; Hauet, A. Multiscale experimental investigations about the cyclic behavior of the 304L SS. *Int. J. Plast.* **2009**, *25*, 1359–1385. [CrossRef]
25. Bocher, L.; Delobelle, P.; Robinet, P.; Feaugas, X. Mechanical and microstructural investigations of an austenitic stainless steel under non-proportional loadings in tension-torsion-internal and external pressure. *Int. J. Plast.* **2001**, *17*, 1491–1530. [CrossRef]
26. Feaugas, X.; Gaudin, C. Ratcheting process in the stainless steel AISI 316L at 300 K: An experimental investigation. *Int. J. Plast.* **2004**, *20*, 643–662. [CrossRef]
27. Gaudin, C.; Feaugas, X. Cyclic creep process in AISI 316L stainless steel in terms of dislocation patterns and internal stresses. *Acta Mater.* **2004**, *52*, 3097–3110. [CrossRef]
28. Cheng, X.; Wang, H.; Kang, G.; Dong, Y.; Liu, Y. Study on strain-induced martensite transformation of 304 stainless steel during ratcheting deformation. *Acta Metall. Sin. Chin. Ed.* **2009**, *45*, 830–834.
29. Dong, Y.; Kang, G.; Liu, Y.; Wang, H.; Cheng, X. Dislocation evolution in 316 L stainless steel during multiaxial ratcheting deformation. *Mater. Charact.* **2012**, *65*, 62–72. [CrossRef]
30. Dong, Y.; Kang, G.; Liu, Y.; Jiang, H. Multiaxial ratcheting of 20 carbon steel: Macroscopic experiments and microscopic observations. *Mater. Charact.* **2013**, *83*, 1–12. [CrossRef]
31. Dong, Y.; Zhang, Z.; He, X. Microscopic substructures of stainless steel 304 undergoing a uniaxial ratcheting deformation. *Acta Mech.* **2020**, *231*, 4919–4931. [CrossRef]
32. Kang, G.; Dong, Y.; Liu, Y.; Wang, H.; Cheng, X. Uniaxial ratcheting of 20 carbon steel: Macroscopic and microscopic experimental observations. *Mater. Sci. Eng. A* **2011**, *528*, 5610–5620. [CrossRef]
33. Kang, G.; Dong, Y.; Wang, H.; Liu, Y.; Cheng, X. Dislocation evolution in 316L stainless steel subjected to uniaxial ratcheting deformation. *Mater. Sci. Eng. A* **2010**, *527*, 5952–5961. [CrossRef]
34. Zhao, W.J. *Cyclic Constitutive Model of High-Speed Railway Train Axle Steel EA4T and Finite Element Implementation*; Hunan University: Hunan, China, 2021; pp. 14–26.
35. Shao, C.W.; Zhang, P.; Liu, R.; Zhang, Z.J.; Pang, J.C.; Zhang, Z.F. Low-cycle and extremely-low-cycle fatigue behaviors of high-Mn austenitic TRIP/TWIP alloys: Property evaluation, damage mechanisms and life prediction. *Acta Mater.* **2016**, *103*, 781–795. [CrossRef]

Disclaimer/Publisher's Note: The statements, opinions and data contained in all publications are solely those of the individual author(s) and contributor(s) and not of MDPI and/or the editor(s). MDPI and/or the editor(s) disclaim responsibility for any injury to people or property resulting from any ideas, methods, instructions or products referred to in the content.